Int. J. Electrochem. Sci., 15 **(2020)** 5193 – 5207, doi: 10.20964/2020.06.16

International Journal of
ELECTROCHEMICAL
SCIENCE
www.electrochemsci.org

Comparative Study on the Corrosion Behaviours of High-Silicon Chromium Iron and Q235 Steel in a Soil Solution

Kechen Lv[1], *Song Xu*[2], *Lanlan Liu*[3], *Xinming Wang*[1], *Cong Li*[1], *Tangqing Wu*[1, *], *Fucheng Yin*[1]

[1] Key Laboratory of Materials Design and Preparation Technology of Hunan Province, School of Materials Science and Engineering, Xiangtan University, Xiangtan 411105, China;
[2] Electric Power Research Institute, State Grid Hunan Electric Power Co. Ltd, Changsha 410007, China;
[3] Maintenance Company, State Grid Hunan Electric Power Co. Ltd, Changsha 410100, China
[*]E-mail: tqwu@xtu.edu.cn

Received: 11 November 2019 / *Accepted:* 8 January 2020 / *Published:* 10 May 2020

High-silicon chromium iron (HSCI) has been applied in grounding grids for some DC converter stations. However, there is a lack of experimental studies on its corrosion behaviour in a soil environment. In this paper, the corrosion behaviours of HSCI and Q235 steel in a soil solution were studied by optical microscopy, electrochemical measurements, SEM/EDS and 3D ultra-depth microscopy. The results show that the anode and cathode polarization branches of HSCI and Q235 steel are mainly dominated by electrochemical polarization. The corrosion resistance of HSCI is much better than that of Q235 steel in the soil solution. The high content of Cr and Si is beneficial for the high corrosion resistance of HSCI; however, the original defects in HSCI promote its corrosion process. Therefore，the reduction of number of the original defects may be conducive to further improving the corrosion resistance of HSCI.

Keywords: High-silicon chromium iron (HSCI); Q235 steel; electrochemical impedance spectroscopy (EIS); polarization curve

1. INTRODUCTION

To meet the demands of low-energy and high-efficiency, power systems are being developed towards combining ultrahigh voltage and excellent capacity over long-distances; however, the above puts forward difficult requirements for the safe operation of the power grid [1]. Grounding devices are an important structure for ensuring the safe operation and reliable power supply of a power grid [2-3]. In actual engineering, some grounding devices are buried in a soil solution and frequently, which may frequently threaten the power system due to the soil solution promoting corrosion [4-5]. In 2008, the potential of a neutral point in a 330 kV substation in Xi'an (China) abnormally increased, inducing the failure of the direct current system of the substation and finally resulting in a large-scale power outage. The subsequent failure analysis confirmed that the internal corrosion of the grounding grid caused an improper grounding of the neutral point.

Copper, carbon steel and galvanized steel are frequently used as grounding electrode materials [6-11]. Although copper is a good grounding material because of its minor contact potential difference and low corrosion rate, its high price and heavy metal pollution hinder its widespread use. Q235 steel has good electrical conductivity and processing properties, but it suffers from serious soil corrosion, which restricts its application in grounding devices [12]. Notably， zinc coatings on steels can block the diffusion of corrosive ions into the steel surface and act as sacrificial anodes to control steel corrosion once the coatings are partially broken [13-15]. Therefore, galvanized steel is a common material used in grounding devices [16]. However, the galvanized layer suffers quick corrosion in acidic and alkaline soils, which induces pitting in the base steel and thus results in potential threats to the grounding devices [17]. Overall, the existing common materials cannot fully meet the needs of grounding devices.

Developing new materials with high resistance-reducing efficiency and low cost is one of the essential development tendencies for grounding devices [18-20]. Omurtag found that Si dioxide will form on a surface of high-silicon cast iron once the Si content increases to 14 wt.%, and the dioxide is able to increase the corrosion resistance of the cast iron [21]. Unfortunately, the high corrosion resistance of high silicon cast iron is reported to be easily ruined by ambient temperatures that are too high or too low [22]. An addition of Cr addition in cast iron is deemed to improve its corrosion resistance, but reduces its toughness and increases its sensitivity to brittle fracture [23]. Karantzalis confirmed that the impact toughness of cast iron decreases with increasing Cr content, while its hardness first increases and then subsequently decreases [24]. On account of the above results, some scholars have developed a new material, which has been named high-silicon chromium iron (HSCI), by simultaneously adding high contents of Cr and Si into cast iron. Electrolytic and mechanical experiments certify that HSCI has strong corrosion resistance and that its mechanical properties can satisfy the needs of grounding devices. Recently, HSCI has been applied in the grounding grid of some DC converter stations in Hunan Province. However, as far as we know, there is no experimental study on the corrosion behaviour of HSCI in a real soil environment; thus, it is impossible to predict its corrosion resistance and lifetime in the ground. For the safety of the grounding device, it is significant to study the corrosion behaviour of HSCI in the soil environment and compare its corrosion resistance with the other common grounding materials mentioned above.

In this paper, the corrosion behaviours of HSCI and Q235 steel in a simulated near-neutral pH soil solution are studied by optical microscopy, electrochemical measurements, SEM/EDS and 3D ultra-depth microscopy. The difference in the corrosion process between HSCI and Q235 steel are compared and the results are beneficial for the selection of grounding device materials in practice.

2. EXPERIMENTAL

2.1 Material

The chemical compositions (wt.%) of the Q235 steel used in the experiment are as follows: C 0.30, P 0.019, S 0.029, Si 0.01, Mn 0.42 and Fe balance. The chemical compositions (wt.%) of HSCI are

C <1.4, Si 15.0, Cr 4.20, Mn 0.50, P 0.20, S 0.09, Mo 0.15, Cu 0.40 and Fe balance. The materials were machined into 10 mm×10 mm×5 mm specimens by the wire cutting. The specimens were welded with copper wires and sealed by epoxy resin, leaving an area of 10 mm×10 mm for the electrochemical measurements. After that, the working surfaces of the specimens were abraded and polished to a mirror-like finish and sequentially cleaned with ethanol and acetone. Then, the specimens were dried by cold air and stored in a desiccator for use.

A near-neutral pH soil solution was used to simulate a neutral soil environment in this work. The chemical composition of the soil solution was $NaHCO_3$ 0.483 g L^{-1}, KCl 0.122 g L^{-1}, $CaCl_2$ 0.127 g L^{-1} and $MgSO_4{\cdot}7H_2O$ 0.131 g L^{-1} [25]. Its pH was adjusted to 7.0~7.2 by 0.1 mol L^{-1} NaOH. The soil solution was prepared with analytical reagents and deionized water.

2.2 Experimental procedure

Prior to the experiment, 1 L of the soil solution was transformed into a jar, and pure N_2 was blown through the jar for 2 h to remove the dissolved oxygen in the soil solution. Then, the HSCI and the Q235 steel specimens were immersed in the jar, and the jar was sealed with silica gel. After that, pure N_2 was again blown through the jar for 2 h to remove any residual oxygen from the soil solution. Three parallel experiments were conducted to ensure the veracity of the experimental data.

The experiments were conducted at room temperature (25±2℃) for 720 h. During the experiment, electrochemical measurements were carried out specific at intervals. After the experiment, the specimen surfaces were characterised via SEM/EDS and 3D ultra-depth microscopy.

2.3 Electrochemical measurement

All the electrochemical measurements were conducted on a CS350 electrochemical measurement system. A three-electrode cell was used for the electrochemical measurements in this work. The Q235 steel or HSCI samples were used as the working electrode, a saturated calomel electrode (SCE) used as the reference electrode and a Pt sheet acted as the counter electrode. The voltage range for the potentiodynamic polarization curves was from −250 mV to +250 mV (vs. OCP) with a scan rate of 1 mV s^{-1}. For cathode cycle polarization curve, the voltage was first scanned from 0 mV to -1500 mV and then returned to 0 mV (vs. OCP). The scan rate for the cathode cycle polarization curve was 10 mV s^{-1}. The fitting and analysis of the polarization curve data were conducted via Origin 8.0 software. Electrochemical impedance spectroscopy (EIS) was used to study the evolution of the corrosion process during the 720 h immersion. Its frequency range was 10^5~10^{-2} Hz and the amplitude of the sinusoidal signal was 10 mV. All EIS data were processed and analysed by Zsimpwin software.

2.4 Surface characterization

After the 720 h immersion, the specimens were taken from the jar, washed with deionized water and ethanol then dried by pure N_2. The morphologies of the corrosion products on the specimen surfaces were observed by scanning electron microscopy (SEM, Zeiss EVO), and the compositions of corrosion products were analyzed by energy dispersive spectrometer (EDS, OXFORD X-Max^N). After that, the corrosion products on the specimen surfaces were removed by a mixture of 500 ml HCl, 500 ml H_2O and 3.5 g hexamethylenetetramine and then the specimens were cleaned with ethanol and dried quickly. The corrosion morphology of the specimens was observed by SEM, and the fluctuation of the corrosion morphology was quantitatively characterized via 3D ultra-depth microscopy (VHX-2000).

3. RESULTS

3.1 Polishing morphology

The morphologies of Q235 steel and HSCI after polishing are shown in Fig. 1. The Q235 steel surface is smooth with some tiny inlad defects (Fig. 1a). Many obvious defects are unevenly distributed on the HSCI surface (Fig. 1b). The area and the number of defects on the HSCI surface are larger than those on the Q235 steel surface. Moreover, the shape of the defects on the HSCI surface is irregular, with sharp shape-changing edges (Fig. 1b).

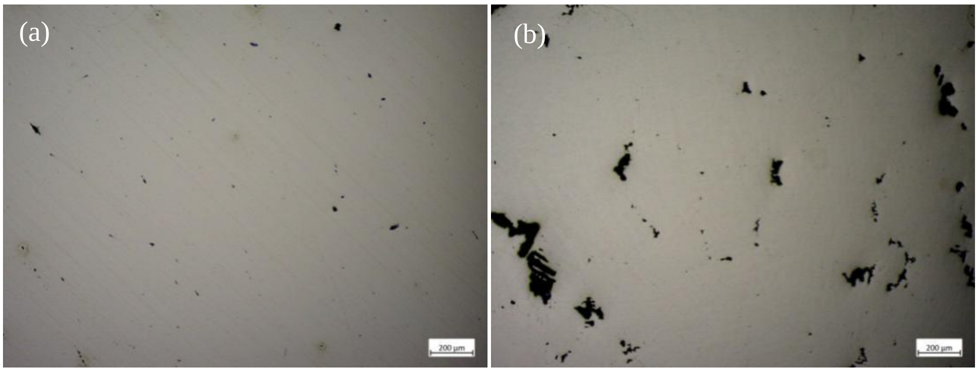

Figure 1. Morphologies of Q235 steel (a) and HSCI (b) after mechanical polishing

3.2 Microtopography of the corrosion products

The micromorphologies of the corrosion products on the Q235 steel and HSCI surfaces after being immersed for the 720 h in a near-neutral pH soil solution are presented in Fig. 2, and the corresponding EDS results are shown in Table 1. The corrosion products on the Q235 steel surface have a layered structure (Fig. 2c). The upper layer of the corrosion products is relatively loose and unevenly distributed, while the lower layer of the corrosion products is porperly dense and complete (Fig. 2e). EDS results demonstrate that the main components of the corrosion products are mainly iron oxide.

After 720 h of immersion, the HSCI surface is covered with a flat and intact corrosion product film (Fig. 2b). The product film is so thin that it can barely be observed in the magnified image (Fig. 2f).

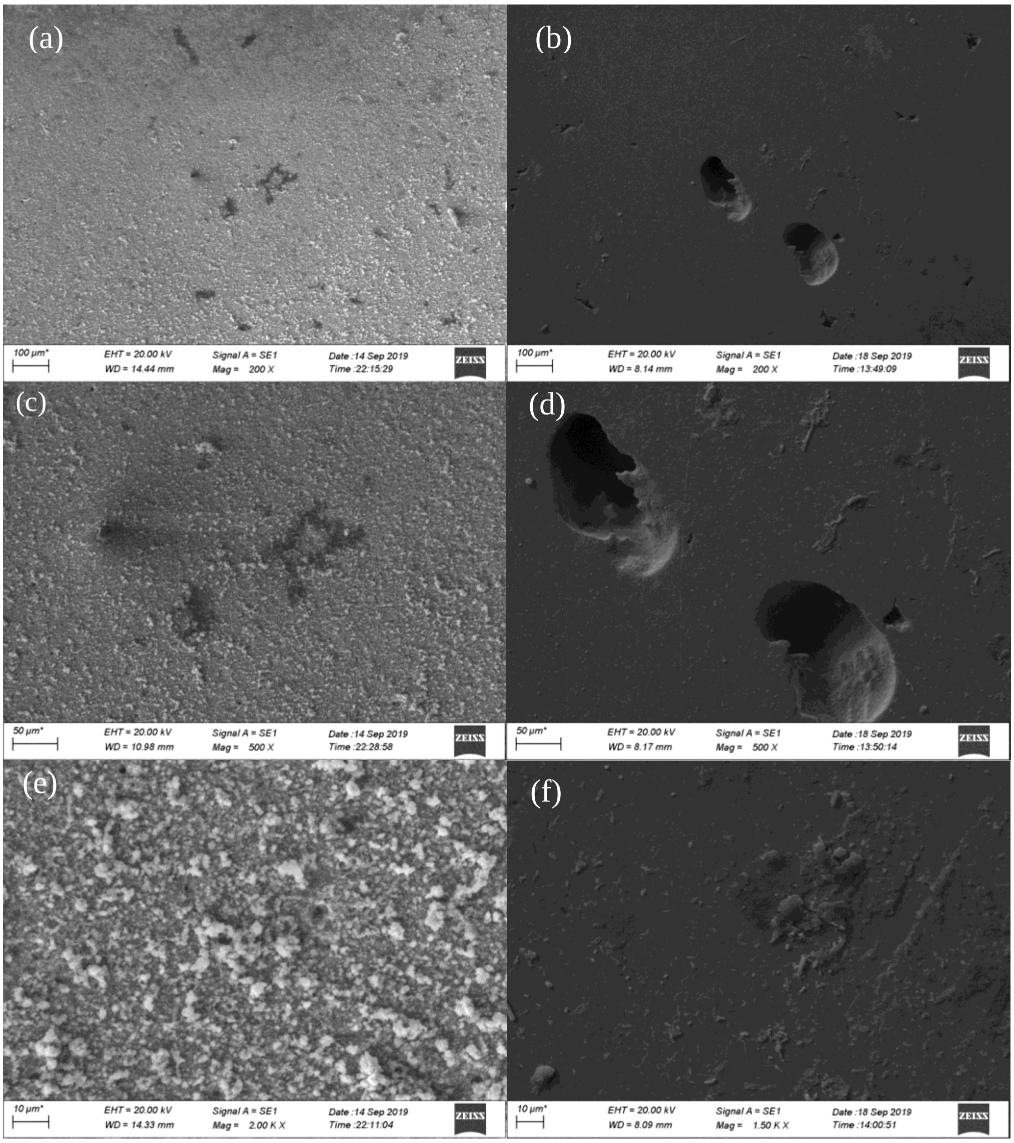

Figure 2. Micromorphologies of the corrosion products on the Q235 steel (a, c, e) and HSCI (b, d, f) surfaces after the 720 h immersion in a near-neutral pH soil solution

Table 1. EDS results of the corrosion products on Q235 steel and HSCI surfaces (at. %)

Position	Fe	O	Na	K	Cl	Ca	Mn	Mg	Si	Cr
A	72.00	26.34	0.57	0.36	0.31	0.22	0.10	0.10	/	/
B	68.35	29.32	0.41	0.29	0.34	0.17	0.10	0.10	0.92	/
C	67.17	30.84	0.24	0.22	0.24	0.15	/	0.03	1.11	/
D	83.70	6.38	0.09	0.01	0.29	/	1.35	/	3.01	5.17
E	64.13	17.30	0.31	1.43	0.11	0.27	0.27	0.26	12.13	3.72
F	51.72	32.80	0.75	3.53	0.44	1.19	0.08	0.42	7.02	1.99

There are many elliptical holes on the HSCI surface with a size of approximately 120 μm×50 μm, but no corrosion product accumulates in the holes (Fig. 2d). Comparing the HSCI surface after immersion with that after polishing (Figs. 1 and 2), it is reasonable to speculate that the elliptical holes may develop from the original defects. During the 720 h immersion, the defect edge becomes significantly smooth, which may be caused by the corrosion and dissolution of the sharp shape-changing edges. EDS results prove that the main corrosion products on the HSCI surface are Fe oxides, Si oxides and Cr oxides.

3.3 Corrosion morphology

The morphologies of corrosion attack on the Q235 steel and HSCI after 720 h of immersion in a near-neutral pH soil solution are presented in Fig. 3. The corrosion morphology of the Q235 steel is flat and uniform, with a distribution of only a few sporadic corrosion pits with diameters of 10~50 μm. The HSCI surface is covered with obvious holes, whose size and shape are similar to the holes in Fig. 2d. These holes may develop from the original defects (Fig. 1b), as discussed in section 3.2. Beyond the holes on the surface, the polishing scratches are very clear, as shown Fig. 3d, which indicates that the corrosion degree of the HSCI surface is extremely shallow. The results demonstrate that the HSCI corrosion is mainly concentrated on the places with sharp shape-changing edges around the holes, but not its entire surface.

To further study the morphologies of corrosion attack on Q235 steel and HSCI, their 3D morphologies are presented in Fig. 4. The maximum pitting depth on the corrosion attack surface is 11.86 μm for the Q235 steel, and the areas beyond the pits suffer from obvious corrosion damage (Fig. 4a). The corrosion of the Q235 steel is not absolutely uniform in the near-neutral pH soil solution. The edge of the hole on the HSCI surface becomes smooth, and some sharply changing structures on the edge disappeared after the 720 h immersion (Fig. 4b). However, the area beyond the holes is extremely flat, indicating that the main corrosion process may take place around the original defects, especially at the sharply changing structures at the defect edges. The above results are similar to the SEM results.

The unique corrosion behaviours of the HSCI surface may be related to the interaction of the complicated shape changing edges and the high contents of Si and Cr in HSCI. Once HSCI is exposed to the soil solution, oxides of Si and Cr may rapidly generate on its surface, which can hinder the diffusion of corrosive ions into the steel surface. However, the shape change of the original hole edges is drastic; thus, it may be difficult for a stable corrosion product films to form on the complicated shape changing edges. Therefore, the edges of the holes become relatively smooth after the 720 h of immersion in the soil solution.

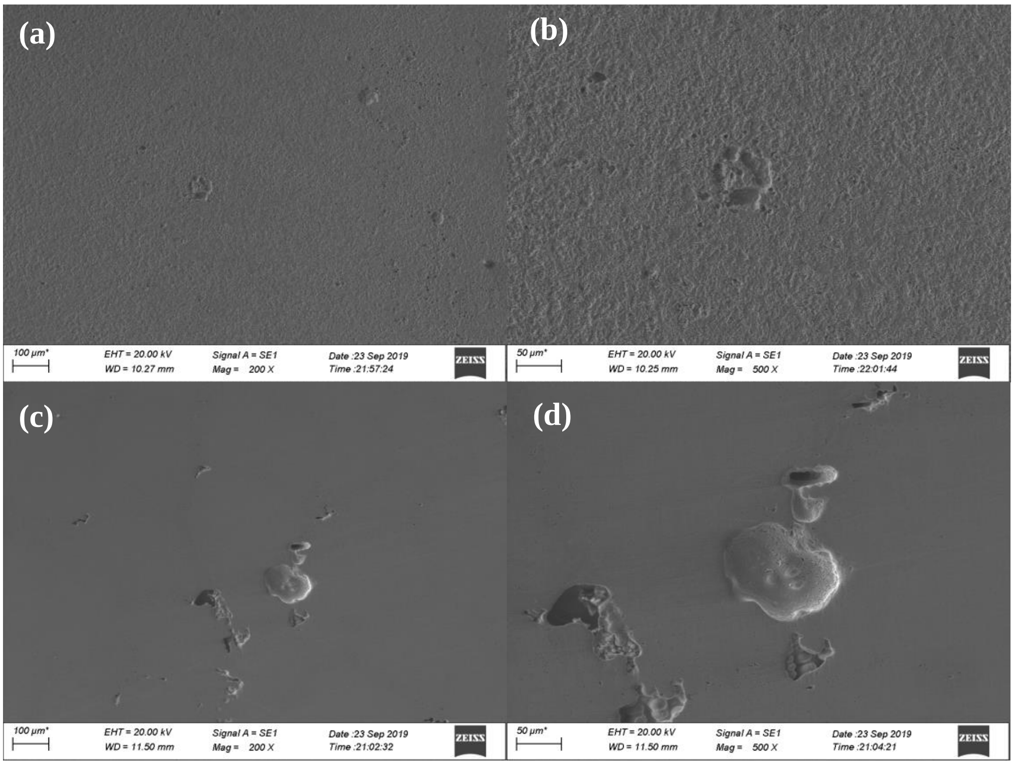

Figure 3. Corrosion attack morphologies of the Q235 steel (a, b) and HSCI (c, d) after the 720 h immersion in a near-neutral pH soil solution

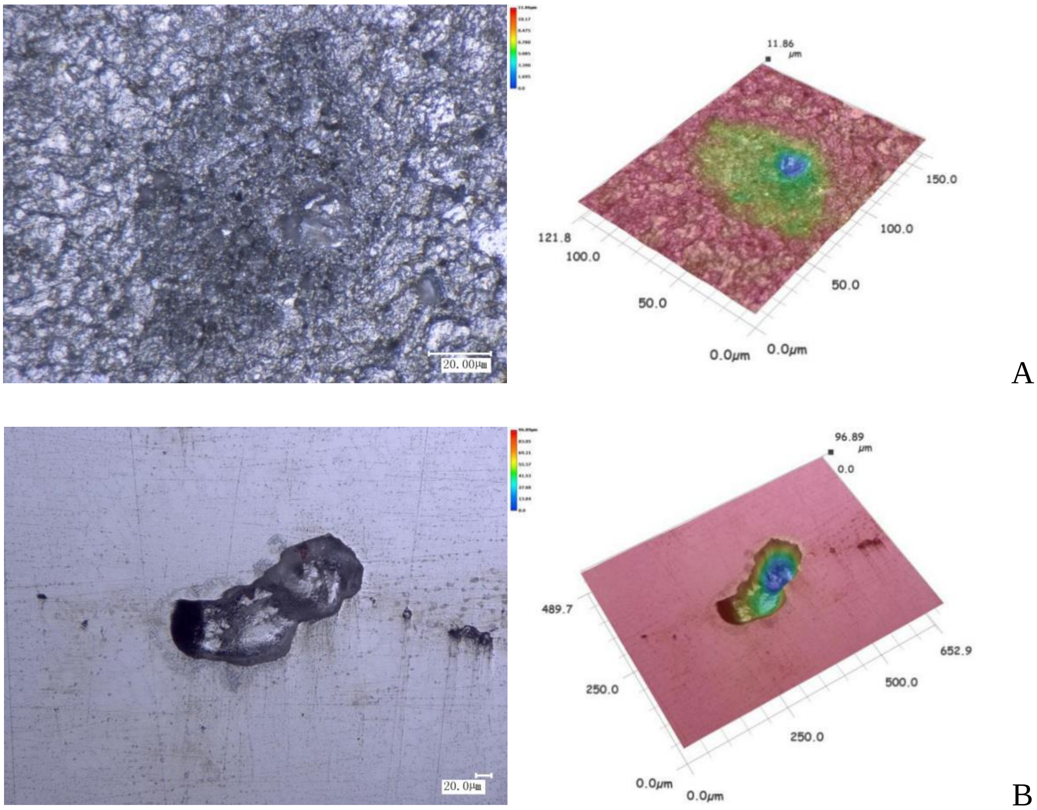

Figure 4. 3D morphologies of the corrosion attack surface of Q235 steel (a) and HSCI (b) in a near-neutral pH soil solution

3.4 EIS

Nyquist and Bode plots of the Q235 steel and HSCI in a near-neutral pH soil solution during the 720 h immersion are shown in Fig. 5. The Nyquist plots of the Q235 steel and HSCI are all similar to compressed capacitive arcs. The radii of the capacitive arcs decrease from the 24th h to the 96th h. After that, the radii of the capacitive arcs increase, and then decrease slightly at the end stage of the immersion. Throughout the immersion, the radius of the capacitive arc for HSCI is always larger than that in Q235 steel, indicating that the corrosion rate of Q235 steel is invariably higher than that of HSCI. In addition, only two time-constants can be observed in the Bode plots of Q235 steel (Fig. 5b), while an additional time constant is presented in the middle frequency range for HSCI (Fig. 5d). This may be related to the passivation property of the Cr and Si oxides corrosion products on the HSCI surface.

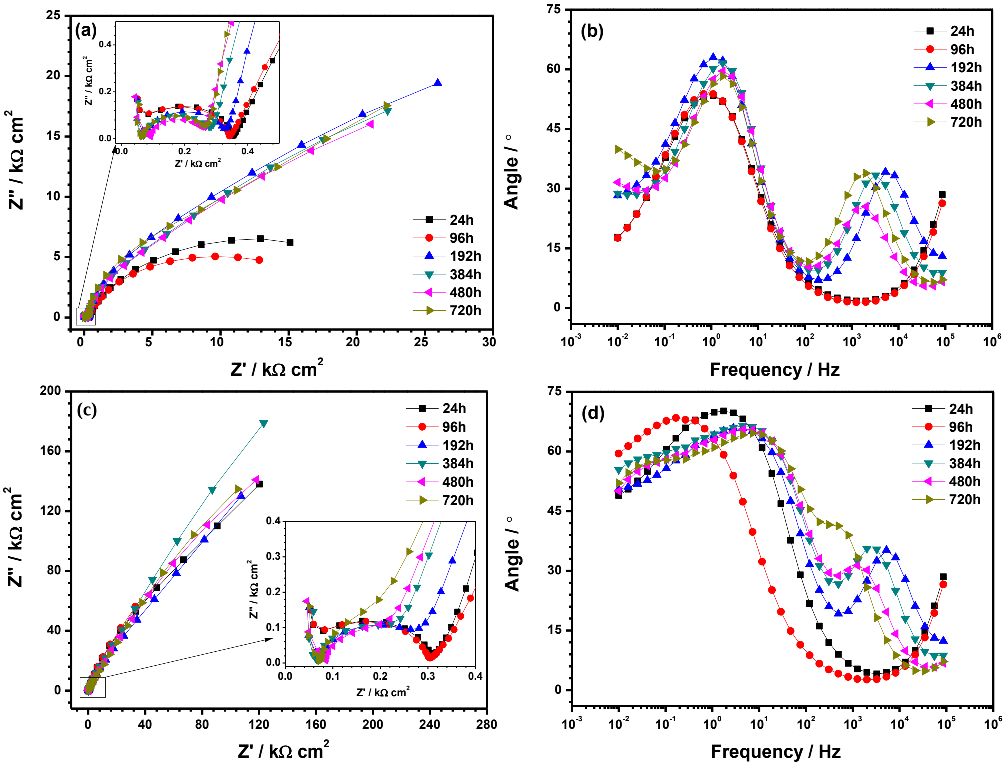

Figure 5. Nyquist and Bode plots of Q235 steel (a, b) and HSCI (c, d) after the 720 h immersion in a near-neutral pH soil solution

3.5 Polarization curves

Potentiodynamic polarization curves of Q235 steel and HSCI after immersion in a soil solution for 12 h and 720 h are presented in Fig. 6. The corrosion potential (E_{corr}), corrosion current density (i_{corr}), cathodic slope (b_c), anodic slope (b_a) and polarization resistance (R_p) are obtained by a straight-line extrapolation and are listed in Table 2 [26-28]. The anode and cathode polarization branches of Q235 steel and HSCI are mainly dominated by electrochemical polarization. The E_{corr} and b_a values of HSCI are higher and larger than those of Q235 at the same time, which may be due to the high contents of the

Cr and Si oxides on the HSCI surface. The above results in a lower i_{corr} and higher R_p of HSCI compared with those of the Q235 steel, as shown in Table 2.

The relatively low i_{corr} and high R_p of HSCI are related to its high content of Cr and Si. During immersion, Cr and Si on the HSCI surface are oxidized into Cr oxide and Si oxide, preventing HSCI surface corrosion. In addition, the additional time constant for HSCI may be related to the corrosion products on the HSCI sueface, indicating the passivation property of the Cr and Si oxides. In addition, as shown from the surface under corrosive attack (Figs. 3 and 4), the corrosion processes of HSCI are mainly concentrated on the complicated shape changing edges around the original defects. Therefore, its apparent corrosion current density is relatively low.

Cyclic polarization curves of the Q235 steel and HSCI after immersing in a near-neutral pH soil solution for 12 h and 720 h are presented in Fig. 7. After cathodic polarization, the E_{corr} values of all the specimens move towards the negative direction, forming a transient E_{corr} [29-30]. When the polarization potential returns to the original E_{corr}, the corresponding current density reaches a new value i_{re}. This result indicates that the effect of cathodic polarization on the metal/solution interface is irreversible.To compare the effect of cathodic polarization on the corrosion process of Q235 steel and HSCI, two parameters, potential drop E_{drop} and additional current i_{add}, were extracted from the cyclic polarization curves. E_{drop} is the difference between the original and transient E_{corr} of the specimen, and i_{add} is the difference between i_{re} and i_{corr}.T E_{drop} and i_{add} can be used to characterize the effect of cathodic polarization on the metal/solution interface and the interface reaction.The E_{drop} values and i_{add} calculated from the polarization curves are also presented in Table 2.

The E_{drop} and i_{add} values of Q235 steel at 720 h doub in a sharp increase compared with those at 12 h, respectively. The above results indicate the enhancing effects of cathodic polarization on the interfacial reaction of Q235 steel over time. The i_{add} of HSCI at 720 h greatly increases compared with that at 12 h, while no obvious change occurs in its E_{drop}. In addition, the E_{drop} of HSCI is larger than that of Q235 steel at both 12 h and 720 h, while the i_{add} of HSCI is less than that of Q235 steel. The above facts demonstrate that the effect of cathodic polarization on corrosion potential is larger than that on corrosion density for the HSCI sample. The above may be related to the oxides on the HSCI surface. According to the EDS results, only Fe oxide exists on the Q235 steel surface, yet a mixture of Fe, Cr and Si oxides are generated in the corrosion product film on the HSCI surface. Given that Cr and Si oxides possess protection and passivation characteristics, we can reasonably speculate that cathodic polarization degrades their protection and passivation properties and results in the larger E_{drop} for HSCI. When the polarization potential returns and hence exceeds the transient E_{corr}, the anodic reaction takes place on the specimen again, and a new corrosion product is instantly generated on the specimen surface. The newly formed mixture of Fe, Cr and Si oxides may effectively compensate for the deterioration of the protection and passivation properties of HSCI; thus, the i_{add} of HSCI is less than that of Q235 steel during immersion.

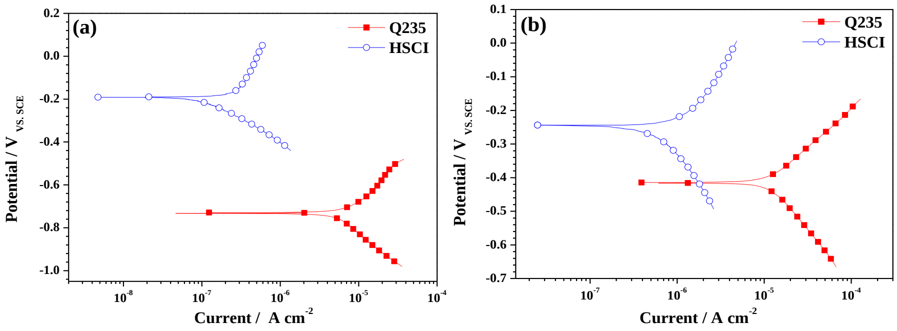

Figure 6. Potentiodynamic polarization curves of Q235 steel and HSCI after immersing in the near-neutral pH soil solution for 12 h (a) and 720 h (b)

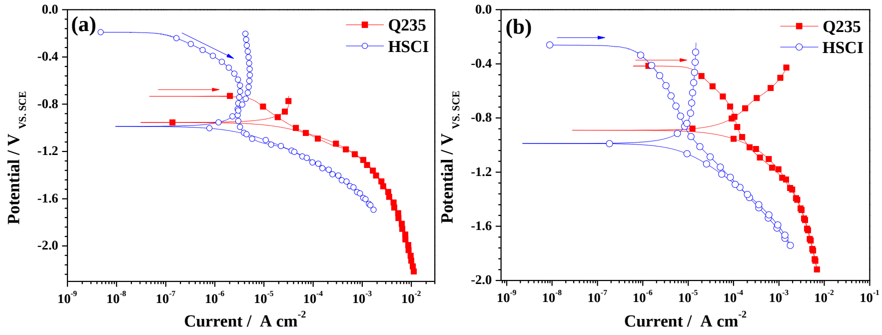

Figure 7. Cyclic polarization curves of Q235 steel and HSCI after immersing in a near-neutral pH soil solution for 12 h (a) and 720 h (b)

Table 2. Fitting results of polarization curves of Q235 steel and HSCI

Time	Specimen	E_{corr} V VS SCE	i_{corr} µA cm^{-2}	b_a mV dec^{-1}	b_c mV dec^{-1}	R_p kΩ cm^2	E_{drop} V	i_{re} µA cm^{-2}	i_{add} µA cm^{-2}
12h	Q235	-0.738	6.399	341	342	11.6	-0.217	32.1	25.7
	HSCI	-0.192	0.224	574	303	385.9	-0.796	4.2	3.9
720h	Q235	-0.416	11.647	231	310	4.9	-0.475	1520.0	1508.0
	HSCI	-0.261	0.949	332	492	90.8	-0.727	14.8	13.9

4. DISCUSSION

4.1 EIS Analysis

Once a metal is immersed in the soil solution, a corrosion reaction instantly takes place and results in the accumulation of corrosion products on its surface. After that, the corrosion processes are affected by both the migration process in the corrosion product film and the charge transfer process in the electric double layer [31]. The corrosion of Q235 steel runs according to the pattern, and a two-constant equivalent circuit is frequently used to characterize this corrosion process (Fig. 8a) [32-33]. In the equivalent circuit, R_s is the solution resistance, R_f and Q_f are the resistance and capacitance of the corrosion product film, respectively; C_{dl} is the capacitance of the double layer and R_{ct} is the charge transfer resistance. As stated in section 3.5, Si and Cr oxides are contained in the corrosion products on the HSCI surface, and they may tend to deposit on and closely combine with the surface, which is similar to a passivation membrane. This speculation can be demonstrated by the high b_a and high R_p of HSCI (Fig. 6 and Table 2). The additional constant in the HSCI Bode plots may be the reflection of the special oxide film. Therefore, a three-constant equivalent circuit is applied to study the corrosion process of HSCI in the work (Fig. 8b) [34]. In the equivalent circuit, C_f is the resistance of the corrosion product film, and R_{pf} and Q_{pf} are the resistance and capacitance of the special oxide film with passivation properties, respectively.

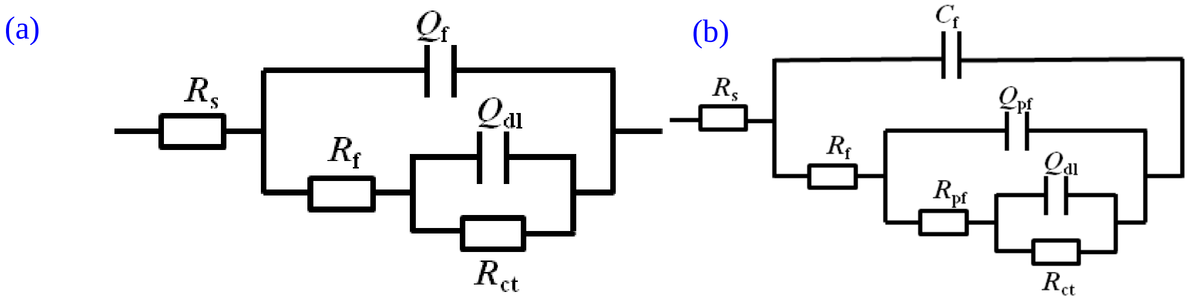

Figure 8. Equivalent circuits used to fit EIS data
(R_s—solution resistance, R_f—resistance of corrosion product film, Q_f/C_f—capacitance of corrosion product film, C_{dl}—capacitance of double layer, R_{ct}—charge transfer resistance, R_{pf}—resistance of Cr and Si oxide film, Q_{pf}—capacitance of Cr and Si oxide film)

EIS fitting results of Q235 steel and HSCI in a soil solution are listed in Table 2 and Table 3, respectively. The R_s values of both Q235 steel and HSCI are distributed in a range of 50~90 Ω cm^2 during the 720 h immersion, and their R_f fluctuates within a range of 150~310 Ω cm^2 [35-36]. The differences in R_s and R_f in the two specimens throughout immersion are relatively limited. However, the R_{pf} of HSCI is distributed in a range of 91~303 kΩ cm^2, which is much greater than the values of R_s and R_f. These results indicate that the oxide film with passivation properties plays a significant role in impeding the corrosion process. In addition, the R_{pf} of HSCI occasionally fluctuates with time, reflecting the fluctuation of the impedance role of the film during immersion. The fluctuation is relative to the fracture and repair of the local oxide on the HSCI surface [37].

R_{ct} is one of the best indicators to reflect the corrosion rate of metal in the EIS fitting results [38-39].The R_{ct} evolutions of Q235 steel and HSCI in the soil solution are presented in Fig. 8. The R_{ct} values of the two specimens decrease with time at the beginning of the experiment, which may result from the combined oxidation-effect of the residual oxygen in the soil solution and the newly-generated ferric oxides on the specimen/solution interface. After that, the corrosion products gradually accumulate on the specimen surface and hinder the migration of corrosive ions into the interface, resulting in a gradual increase of R_{ct} from the 100th h to the 480th h. At the last stage of immersion, the R_{ct} value decreases slightly until the end of the experiment.

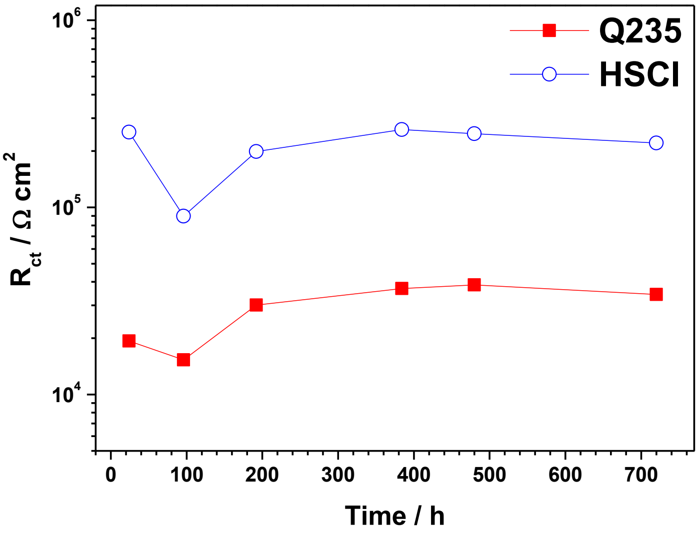

Figure 9. R_{ct} evolutions of Q235 steel and HSCI in a near-neutral pH soil solution as a function of time

Table 2. Fitting results of EIS of Q235 steel in a soil solution

Time h	R_{s} $\Omega\cdot\mathrm{cm}^2$	Y_{f} $\mathrm{S\cdot sec^n\cdot cm^{-2}}$	n_{f}	R_{f} $\Omega\cdot\mathrm{cm}^2$	Y_{dl} $\mathrm{S\cdot sec^n\cdot cm^{-2}}$	n_{dl}	R_{ct} $\Omega\cdot\mathrm{cm}^2$	X^2
24	50.57	4.507×10^{-9}	0.9650	296.3	1.607×10^{-4}	0.7332	1.931×10^{4}	1.642×10^{-3}
96	54.71	6.332×10^{-9}	0.9749	282.4	1.677×10^{-4}	0.7461	1.531×10^{4}	1.663×10^{-3}
192	56.32	4.796×10^{-9}	0.9957	255.9	1.280×10^{-4}	0.7786	3.009×10^{4}	6.199×10^{-3}
384	69.14	5.329×10^{-7}	0.9813	197.6	1.320×10^{-4}	0.7752	3.681×10^{4}	1.301×10^{-2}
480	90.57	7.888×10^{-7}	1.0000	152.7	1.388×10^{-4}	0.7672	3.852×10^{4}	1.348×10^{-3}
720	65.26	1.076×10^{-6}	0.9757	193.5	1.280×10^{-4}	0.8218	3.430×10^{4}	1.363×10^{-2}

Table 3. Fitting results of EIS of HSCI in a soil solution

Time h	R_{s} $\Omega\cdot\mathrm{cm}^2$	C_{f} $\mathrm{F\cdot cm^{-2}}$	R_{f} $\Omega\cdot\mathrm{cm}^2$	Y_{pf} $\mathrm{S\cdot sec^n\cdot cm^{-2}}$	n_{pf}	R_{pf} $\Omega\cdot\mathrm{cm}^2$	Y_{dl} $\mathrm{S\cdot sec^n\cdot cm^{-2}}$	n_{dl}	R_{ct} $\Omega\cdot\mathrm{cm}^2$	X^2
24	87.35	7.618×10^{-9}	225.2	2.610×10^{-5}	0.8328	1.680×10^{5}	6.484×10^{-5}	1.000	2.525×10^{5}	7.909×10^{-4}
96	90.31	7.391×10^{-9}	219.2	1.158×10^{-4}	0.7929	2.375×10^{5}	2.484×10^{-4}	1.000	8.970×10^{4}	1.204×10^{-3}
192	65.05	5.741×10^{-9}	211.1	2.544×10^{-5}	0.7958	9.188×10^{4}	5.902×10^{-5}	0.9608	1.987×10^{5}	1.536×10^{-3}
384	66.57	5.223×10^{-7}	173.4	2.429×10^{-5}	0.7704	2.150×10^{5}	3.052×10^{-5}	1.000	2.604×10^{5}	4.915×10^{-3}
480	84.08	8.453×10^{-7}	151.7	2.426×10^{-5}	0.7724	1.118×10^{5}	3.107×10^{-5}	1.000	2.479×10^{5}	2.770×10^{-3}
720	73.11	1.735×10^{-6}	155.5	3.014×10^{-5}	0.6996	3.027×10^{5}	3.090×10^{-5}	1.000	2.206×10^{5}	3.669×10^{-3}

At that time, Cl^- and SO_4^{2-} may penetrate through the corrosion product film, inducing the formation of pits on the specimen surface and accelerating the corrosion rates. Throughout the immersion, the R_{ct} of HSCI is higher than that of Q235 steel, indicating the higher corrosion resistance of HSCI in the near-neutral pH soil solution. The higher corrosion resistance may stem from the Si content and Cr content in HSCI.

4.2 Corrosion behaviour of HSCI in a near-neutral pH soil solution

From the above results, the corrosion rate of HSCI first increases and subsequently decreases, before slightly increasing at the end stage of the 720 h immersion in a near-neutral pH soil solution. The number of defects on the HSCI surface does not increase during immersion; moreover, the sharp shape-changing structures around the defects are corroded and dissolved, and the edges of the defects become smoother. The above results indicate that HSCI corrosion mainly occurs around the defects in the soil solution. The polarization resistance of HSCI is higher and its corrosion rate is lower than those of Q235 steel, showing the much better corrosion resistance of HSCI compared with Q235 steel in a near-neutral pH soil solution. The corrosion resistance of HSCI is related to its high contents of Cr and Si. During the 720 h immersion, elements such as Fe, Cr and Si dissolved into the soil solution and formed their oxides on the HSCI surface. SiO2 and CrO2 have been reported to possess the good corrosion resistance [40]; thus, their presence increases the corrosion resistance and reduces the corrosion rate of HSCI in a near-neutral pH soil solutions.

The defects on the HSCI surface play a significant role in its corrosion process. As shown in Fig. 1, the geometries of the defects on the HSCI surface are intensely irregular. Due to their sharp shape-changes, it is difficult for an intact oxide film to form on those irregular defects.In addition, in the soil solution, the irregular surface defects increase the contact area between the HSCI surface and the soil solution, resulting in the preferential dissolution of the sharp shape-changing structures around the defects. Therefore, it is reasonable to infer that the defects on the HSCI surface may enhance the corrosion rate of HSCI, which results in relatively smooth edges around the holes after the 720 h of immersion in the soil solution. Thus, the reduction of the number of original defects in HSCI may be conducive to further improving its corrosion resistance.

5. CONCLUSION

The corrosion behaviours of HSCI and Q235 steel in a near-neutral pH soil solution were studied in this work. The conclusions can be summarized as follows:

1. After 720 h of immersion in the near-neutral pH soil solution, a flat and thin corrosion product film covers the HSCI surface and the corrosion process is mainly concentrated on the edges of the original defects on the HSCI surface.

2. The anode and cathode polarization branches of Q235 steel and HSCI are mainly dominated by electrochemical polarization. The corrosion rate of HSCI first increases and subsequently decreases, before slightly increasing at the end stage of the 720 h immersion in a near-neutral pH soil solution.

3. Throughout the 720 h immersion, the polarization resistance of HSCI is higher than that of Q235 steel and its corrosion rate is lower than that of Q235 steel. The corrosion resistance of HSCI is much better than that of Q235 steel in the near-neutral pH soil solution.

4. The high corrosion resistance of HSCI is related to its high contents of Cr and Si. The formed oxide film with passivation properties plays a significant role in impeding the corrosion process of HSCI in the soil solution.

5. The defects on the HSCI surface play a significant role in promoting the corrosion process of HSCI. The reduction of the number of original defects may be conducive to further improving the corrosion resistance of HSCI.

ACKNOWLEDGMENTS

We are grateful for financial support of National Natural Science Foundation of China (51971191, 51601164) and Hunan Provincial Natural Science Foundation of China (2019JJ30023, 2019RS2038).

References

1. D. Paul, *Ieee. T. Iid. Appl.*, 38 (2002) 818.
2. G. Doyle, M.V. Seica and M.W.F. Grabinsky, *Can. Geotech. J.,* 40 (2003) 225.
3. J. Fu, F. Pei, Z. Zhu, Z. Tan, X. Tian, R. Mao and L. Wang, *Anti-Corros. Method. M.,* 60 (2013) 148.
4. V.L. Coelho, A. Piantini and H.A.D. Almaguer, *Electr. Pow. Syst. Res.,*118 (2015) 76.
5. Z. Chen, C. Qin, J. Tang and Y. Zhou, *J. Nat. Gas. Sci. Eng.*, 15 (2013) 76.
6. G. Cui, Z. Li, C. Yang and X. Wei, *Corros. Rev.*, 33 (2015) 233.
7. Z.P. Zhu, X.C. Jiao, X.Y. Tang and H.W. Lu, *Anti-Corros. Method. M.*, 62 (2015) 322.
8. J. Du, J Guo, L. Zhao, Y. Chen, C. Liu and X. Meng, *Int. J. Electrochem. Sci.*, 13 (2018) 5810.
9. H. Liu and Y.F. Cheng, *Corros. Sci.,* 133 (2018) 178.
10. V. Katic, Z. I. Buljan, S. Spalj and H.O. Ćurković, *Int. J. Electrochem. Sci.*, 13 (2018) 4160.
11. Y. Qiao, D. Xu, S. Wang, Y. Ma, J. Chen, Y. Wang, and H. Zhou, *Metals.*, 9 (2019) 1213.
12. Y. Guo, H. Tan, D. Wang and T. Meng, *Anti-Corros. Method. M.*, 64 (2017) 599.
13. R.P Edavan and R. Kopinski, *Corros. Sci.,* 51 (2009) 2429.
14. R. Hausbrand, M. Stratmann and M. Rohwerder, *Corros. Sci.*, 51 (2009) 2107.
15. M.C. Li, M. Royer, D. Stien, A. Lecante and C. Roos, *Corros. Sci.,*50 (2008) 1975.
16. S. Liu, H. Sun, L. Sun and H. Fan, *Corros. Sci.*, 65 (2012) 520.
17. W. Wei, X.Q. Wu, W. Ke, S. Xu, B. Feng and B.T. Hu, *J. Mater. Eng. Perform.*, 25 (2016) 518.
18. R.E. Melchers and T. Wells, *Corros. Eng. Sci. Techn.*, 53 (2018) 524.
19. V.L. Coelho, A. Piantini, H.A. Almaguer, R.A. Coelho, W.D.C. Boaventura and J.O.S. Paulino, *Electr. Pow. Syst. Res.*, 118 (2015) 76.
20. Y. Qiao, J. Chen, H. Zhou, Y. Wang, Q. Song, H. Li and Z. Zheng, *Wear.,* 424 (2019) 70.
21. Y. Omurtag and M. Doruk, *Corros. Sci.*, 10 (1970) 225.
22. G.N. Safronov, N.N. Safronov and L.R. Kharisov, *Chem. Pet. Eng.*, 51 (2015) 142.
23. E. Zumelzu, I. Goyos, C. Cabezas, O. Opitz and A. Parada, *J. Mater. Process. Tech.*, 128 (2002) 250.
24. A.E. Karantzalis, A. Lekatou, and H. Mavros, *J. Mater. Eng. Perform.*, 18 (2009) 174.
25. I.M. Gadala and A. Alfantazi, *Corros. Sci.,* 82 (2014) 45.

26. T. Bellezze, G. Giuliani and G. Roventi, *Corros. Sci.*, 130 (2018) 113.
27. J. Wang and L.F. Zhang, *Anti-Corros. Method. M.*, 64 (2017) 252.
28. Y. Qiao, Z. Tian, X. Cai, J. Chen, Y. Wang, Q. Song and H. Li, *Tribol. Lett.*, 67 (2019) 1.
29. Y. Tang, Y. Zuo, J. Wang, X. Zhao, B. Niu, and B. Lin, *Corros. Sci.*, 80 (2014) 111.
30. F. Mao, C. Dong and D.D. Macdonald. *Corros. Sci.*, 98 (2015) 192.
31. C.N. Cao, Principles of electrochemistry of corrosion, *China Chemistry Press.*, Beijing, 2008.
32. J. Wu, D. Zhang, P. Wang, Y. Cheng, S. Sun, Y. Sun, and S. Chen, *Corros. Sci.*, 112 (2016) 552.
33. J. Zhang, W.W. Song, D.L. Shi, L.W. Niu, C.J Li and M. Du, *Prog. Org. Coat.*, 75 (2012) 284.
34. H. Luo, H. Su, C. Dong and X. Li, *Appl. Surf. Sci.*, 400 (2017) 38.
35. J. Xu, K. Wang, C. Sun, F. Wang, X. Li, J. Yang and C. Yu, *Corros. Sci.*, 53 (2011) 1554.
36. Z. Yu, J. Zhang, X. Zhao, X. Zhao, J. Duan and X. Song, *Int. J. Electrochem. Sci.*, 9 (2014) 7587.
37. G. Okamoto, *Corros. Sci.*, 13 (1973) 47.
38. M.A. Deyab and S.A. El-Rehim, *Int. J. Electrochem. Sci.*, 8 (2013) 12613.
39. S.T. Selvi, V. Raman and N. Rajendran, *J. Appl. Electrochem.*, 33 (2003) 1175.
40. Q. Fu, Y. Shan, S. Wen, H. Li, Y. Chu, and X. Liu, *Corros. Sci.*, 83 (2014) 103.